Magnetic Resonance Images Reconstruction using Uniform Discrete Curvelet Transform Sparse Prior based Compressed Sensing

Bingxin Yang Min Yuan Yide Ma* Jiuwen Zhang
LanZhou University
Tianshui South Road No.222, 730000, LanZhou, China
* Corresponding author
18919849359@163.com yuanm@lzu.edu.cn ydma01@126.com zhangjw@lzu.edu.cn

ABSTRACT

Compressed sensing(CS) has shown great potential in speeding up magnetic resonance imaging(MRI) without degrading images quality. In CS MRI, sparsity (compressibility) is a crucial premise to reconstruct high-quality images from non-uniformly undersampled *k*-space measurements. In this paper, a novel multi-scale geometric analysis method (uniform discrete curvelet transform) is introduced as sparse prior to sparsify magnetic resonance images. The generated CS MRI reconstruction formulation is solved via variable splitting and alternating direction method of multipliers, involving revising sparse coefficients via optimizing penalty term and measurements via constraining *k*-space data fidelity term. The reconstructed result is the weighted average of the two terms. Simulated results on in vivo data are evaluated by objective indices and visual perception, which indicate that the proposed method outperforms earlier methods and can obtain lower reconstruction error.

Keywords

Compressed sensing, magnetic resonance imaging, uniform discrete curvelet transform, variable splitting, alternating direction method of multipliers.

1 INTRODUCTION

Traditional scanning methods of magnetic resonance imaging(MRI) spent plenty of time on data acquisition. This brought negative influences for clinical diagnosis. *K*-space undersampling provides one method to speed up the imaging at the expense of introducing aliasing for violating the Nyquist (Shannon) sampling theorem.

Compressed sensing(CS) [baraniuk2007compressive, 1614066] points out, sparse or compressible signal can be reconstructed precisely from less number of sampled data than those constrained by Nyquist sampling theorem. Hence, CS provides theoretical feasibility for highly undersampled MR images reconstruction. The emerging approach is termed CS MRI [lustig2007sparse, 4472246]. The main principles of CS MRI are that the images to be reconstructed can be sparsely represented; measurement matrix is irrelevant to sparse transform basis; the reconstruction optimization problem can be solved by using nonlinear method. In CS MRI, incoherent random, radial and spiral sampling trajectories are applied to obtain *k*-space measurements [lustig2007sparse, chen2010novel, santos2006single]. The generally employed sparsifying methods include spatial finite-difference [lustig2007sparse, huang2011efficient, huang2012compressed], discrete wavelet transform(DWT) [lustig2007sparse, huang2011efficient, huang2012compressed], multi-scale geometric analysis(MGA) methods (contourlet transform [1532309], nonsubsampled contourlet transform [da2006nonsubsampled], sharp frequency localization contourlet(SFLCT) [lu2006new], discrete curvelet transform using fast algorithm(FDCT) [candes2006fast] and discrete shearlet transform(DST) [lim2010discrete]), dictionary learnt from intermediate reconstruction or fully sampled images [ning2013magnetic, qu2012undersampled], temporal sparsity along temporal axis for dynamic cardiac imaging [bilen2012high] and the combination of some of these transforms [lustig2007sparse, huang2011efficient]. The main thoughts of reconstruction approaches are nonlinearly reconstructing original signal accurately from a small number of measurements. The generally used are greedy pursuit class (matching pursuit, orthogonal

matching pursuit) for solving sparse coefficients l_0 regularization, provided that the sparsity of image is already known; linear programming (gradient projection, basis pursuit) handling sparse coefficients l_1 regularization at the cost of high computational complexity; minimizing non-convex l_p $(0 < p < 1)$ quasi-norm such as the recent one in [candes2008enhancing], which doesn't always give global minima and is also slow. The widely used methods are based on augmented Lagrangian for solving convex, non-smooth regularization (total variation and l_1) optimization. These methods include YALL1 [yang2011alternating], FCSA [huang2011efficient], split augmented Lagrangian shrinkage algorithm(SALSA) [afonso2010fast] and constrained split augmented Lagrangian shrinkage algorithm(C-SALSA) [5570998], etc.

In this paper, a novel MGA method termed uniform discrete curvelet transform(UDCT) (refer to [5443489] for details) is adopted to sparsify MR images. In terms of the alias free subsampling in frequency domain they both employed, UDCT has similar properties as wrapping-based FDCT, such as tight frame property, highly directional sensitivity and anisotropy. Besides, UDCT is superior than FDCT for its lower redundancy of 4 and clear coefficients parent-children relationship. Reconstruction model is proposed involving UDCT coefficients regularization term and k-space data fidelity term. To solve the corresponding reconstruction model, C-SALSA, i.e., variable splitting(VS) and alternating direction method of multipliers(ADMM-2) [5570998] is used. The proposed CS MRI method is termed UDCSMRI.

The paper is organized as follows. Section 2 describes the existing CS MRI work, and then introduces UDCSMRI in detail including UDCT sparse prior and corresponding reconstruction model handling the ill-posed linear inverse problems. In section 3 UDCSMRI is compared with current CS MRI methods in reconstruction performance. Then its ability of handling noise and convergence performance is analyzed. Conclusions and future work involving extending this work to dynamic parallel MRI are explicit in section 4.

2 MATERIALS AND METHODS

CS MRI

Define $\mathbf{x} \in \mathbb{C}^{\mathbf{n}}$ is vector-version of 2D image to be reconstructed. $\mathbf{y} = \mathbf{F_u x}$ denotes undersampling in k-space, where $\mathbf{F_u} \in \mathbb{C}^{\mathbf{m}\times\mathbf{n}}$ means undersampled Fourier Encoding matrix and $\mathbf{y} \in \mathbb{C}^{\mathbf{m}}$ represents k-space measurements. $\mathbf{\Psi} \in \mathbb{C}^{t\times n}$ represents analytical sparse transform matrix or the inverse of a set of learnt signals. CS reconstructs the underlying MR image $\mathbf{x}$ from measurements $\mathbf{y}$ via solving the constrained linear inverse problem, denoted as Eq. (1)

$$\min_{\mathbf{x}} \|\mathbf{\Psi x}\|_1 \text{ s.t. } \|\mathbf{F_u x} - \mathbf{y}\|_2^2 \leq \boldsymbol{\varepsilon} \qquad (1)$$

where $\boldsymbol{\varepsilon} \in \mathbb{C}^m$ controls the allowed noise level in reconstructed image, l_1 enforces sparsity, l_2 constrains the data fidelity. Finite-difference (total variation) is generally added to the objective to suppress the noise and preserve images details simultaneously, then the problem is

$$\min_{\mathbf{x}} \|\mathbf{\Psi x}\|_1 + \beta TV(\mathbf{x}) \text{ s.t. } \|\mathbf{F_u x} - \mathbf{y}\|_2^2 \leq \boldsymbol{\varepsilon} \qquad (2)$$

where $\beta > 0$ denotes weight of total variation(TV). Rather than Eq. (1), most current methods handling linear inverse problems with convex, non-smooth regularization (l_1 and TV) consider the unconstrained problem

$$\min_{\mathbf{x}} \beta_1 \|\mathbf{\Psi x}\|_1 + \beta_2 TV(\mathbf{x}) + \frac{1}{2}\|\mathbf{F_u x} - \mathbf{y}\|_2^2 \qquad (3)$$

in which $\beta_{1(2)} > 0$ is regularization parameter. The commonly used techniques dealing with Eq. (3) are VS and methods upon augmented Lagrangian, such as TVCMRI [ma2008efficient], RecPF, FCSA, SALSA, etc. However, Eq. (3) is not efficient for ignoring $\boldsymbol{\varepsilon}$, which has a clear meaning (proportional to the noise deviation) and is easier to set than parameter $\beta_{1(2)}$. Additionally, numerous different reconstruction models have been explored, such as NLTV-MRI incorporating with nonlocal TV [huang2012compressed], reconstruction upon wavelet tree structured sparsity(WaTMRI) studied in [NIPS20124630], reconstruction by using dictionary learning(DL) [qu2012undersampled, ning2013magnetic] and patch-based nonlocal operator combined with VS and quadratic penalty reconstruction technique named PANO [qu2014magnetic], etc. Besides, 3D dynamic parallel imaging has also been proposed and is of great significance for practical MRI applications. It is established on either sparsity along temporal axis [bilen2012high] or structured low-rank matrix completion [shin2013calibrationless],.

Proposed Method based on UDCT

In this paper, MR images are sparsified by MGA method named UDCT. Efficient C-SALSA is introduced to solve the generated CS MRI reconstruction formulation under UDCT sparse prior. MR image $\mathbf{x}$ to be reconstructed is initialized to one zero-filling image. This zero-filling image is obtained from the result of direct inverse Fourier transform to zero filled k-space measurements, represented as $\mathbf{x_0} = \mathbf{F_u^H y}$. Zero-filling image serves as the original intermediate image. The real and imaginary part of $\mathbf{x_0}$ are decomposed into J levels by using UDCT separately, $2\kappa_j$ directional sub-bands for each level. CS MRI reconstruction problem comes down to solving the optimization problem constrained by image transform sparsity and k-space measurements fidelity (in an iterative process). The solving process requires the definition of the Moreau proximal maps of regularization term and fidelity term.

Reconstruction result is the trade-off between the two terms and then serves as the intermediate image for the next iteration. This procedure is executed iteratively until some stop criterion is satisfied. Framework of UDCSMRI in Fig.1 demonstrates clearly the implementation process.

Uniform Discrete Curvelet Transform

As is known, discrete wavelet basis only represents the location and features of singular point with limited directions. The generally used contourlet transform lacks shift-invariance and brings pseudo-Gibbs phenomena around singular points. NSCT owns too high redundancy and SFLCT cannot capture clear directional features in spite of flexible redundancy. The needle-shaped elements of FDCT allow very high directional sensitivity and anisotropy and are thus very efficient in representing line-like edges. But FDCT possesses too high redundancy, which makes it sub-optimal in sparse representation, either. UDCT has been proposed as an innovative implementation of discrete curvelet transform for real-valued signals. Utilizing the ideas of FFT-based discrete curvelet transform and filter-bank based contourlet transform, UDCT is designed as a perfect multiresolution reconstruction filter bank(FB) but executed by FFT algorithm. The number of UDCT coefficients are fixed at each scale and sizes of directional sub-bands are the same for each scale, which provides simple calculation. UDCT can provide a flexible instead of fixed number of clear directions at each scale to capture various directional geometrical structures accurately. Besides, the forward and inverse transform form a tight and self-dual frame with an acceptable redundancy of 4 to allow the input real-valued signal to be perfectly reconstructed. UDCT has asymptotic approximation properties: for image $\mathbf{x}$ with C^2 (C is a constant) singularities, the best N-term approximation $\mathbf{x_N}$ (N is the number of most important transform coefficients allowing reconstruction) in the curvelet expansion is [candes2000curvelets]

$$\|\mathbf{x}-\mathbf{x_N}\|_2^2 \leq CN^{-2}\left(\log \mathrm{N}\right)^3 \; N \to \infty \tag{4}$$

This property is known as the optimal sparsity. Therefore, UDCT is considered as the preeminent MGA method for CS MRI application.

Constrained Split Augmented Lagrangian Shrinkage Algorithm

Define Φ as regularization function, $\boldsymbol{\Psi}$ the UDCT analytical operator, the sparse representation is defined as $\boldsymbol{\alpha}=\boldsymbol{\Psi}\mathbf{x}$. The reconstruction model can thus be denoted as

$$\begin{aligned}&\min_{\boldsymbol{\alpha},\mathbf{x}} \Phi(\boldsymbol{\alpha}) = \begin{cases}\|\boldsymbol{\alpha}\|_1 & \text{if } \Phi = l_1 \\ TV\left(\boldsymbol{\Psi}^{-1}\boldsymbol{\alpha}\right) & \text{if } \Phi = TV\end{cases} \\ &\text{s.t. } \|\mathbf{F_u x}-\mathbf{y}\|_2^2 \leq \boldsymbol{\varepsilon}\end{aligned} \tag{5}$$

Eq. (5) is solved by C-SALSA. Different from the previous augmented Lagrangian based methods to solve Eq. (3), C-SALSA has been proposed as a new augmented Lagrangian based method, which directly solves the original constrained inverse problem optimization efficiently. C-SALSA first translates the constrained Eq. (5) into an unconstrained one via adding the indicator function of the feasible set, the ellipsoid $\{\mathbf{x} : \|\mathbf{F_u x}-\mathbf{y}\|_2^2 \leq \boldsymbol{\varepsilon}\}$, to the objective in Eq. (5). Then the unconstrained problem can be denoted as

$$\min_{\boldsymbol{\alpha},\mathbf{x}} \lambda_1 \Phi(\boldsymbol{\alpha}) + \lambda_2 \mathscr{L}_{E(\boldsymbol{\varepsilon},\mathbf{I},\mathbf{y})}(\mathbf{F_u x}) \tag{6}$$

In Eq. (6), parameters λ_1 and λ_2 measure the weight of the regularization term and error constraint term, respectively. The values linearly increase along with the increase of iteration number ($\lambda_{1(2)} \leftarrow \rho\lambda_{1(2)}$, $\rho > 1$ means linear growth factor). Eq. (6) is translated into another constrained problem via VS, denoted as

$$\min_{\boldsymbol{\alpha}\in\mathbb{C}^t,\mathbf{x}\in\mathbb{C}^{\mathbf{n}},\boldsymbol{\nu}\in\mathbb{C}^{\mathbf{m}}} \lambda_1 \Phi(\boldsymbol{\alpha}) + \lambda_2 \mathscr{L}_{E(\boldsymbol{\varepsilon},\mathbf{I},\mathbf{y})}(\boldsymbol{\nu}) \text{ s.t. } \boldsymbol{\nu} = \mathbf{F_u x} \tag{7}$$

Finally, ADMM-2 solves the two sub-problems concerning $\boldsymbol{\alpha}$ and $\boldsymbol{\nu}$. The reconstruction result is obtained in this way. In terms of sub-problem concerning the regularization Φ, the Moreau proximal mapping function can be defined as

$$\boldsymbol{\Theta}_{\Phi}\left(\widehat{\boldsymbol{\alpha}}\right) = \arg\min_{\boldsymbol{\alpha}} \frac{1}{2}\left\|\boldsymbol{\alpha}-\widehat{\boldsymbol{\alpha}}\right\|_2^2 + \Phi(\boldsymbol{\alpha}) \tag{8}$$

where $\widehat{\boldsymbol{\alpha}}$ is the result of mapping to $\boldsymbol{\alpha}$ according to the mapping relation $\mathbb{C}^t \to \mathbb{C}^t$. If $\Phi(\cdot) \equiv \|\cdot\|_1$, $\boldsymbol{\Theta}_{\Phi}$ is simply a soft threshold. If Φ is TV norm, Chambolle's algorithm [chambolle2004algorithm] is available to compute the involving problem. $E(\boldsymbol{\varepsilon},\mathbf{I},\mathbf{y})$ represents a closed $\boldsymbol{\varepsilon}$-radius Euclidean ball centered at $\mathbf{y}$. The Moreau proximal map of $\mathscr{L}_{E(\boldsymbol{\varepsilon},\mathbf{I},\mathbf{y})}$ can be simply denoted as the orthogonal projection of $\boldsymbol{\nu}$ on the closed $\boldsymbol{\varepsilon}$-radius ball centered at $\mathbf{y}$

$$\boldsymbol{\Theta}_{\mathscr{L}_{E(\boldsymbol{\varepsilon},\mathbf{I},\mathbf{y})}}(\boldsymbol{\nu}) = \begin{cases}\mathbf{y} + \boldsymbol{\varepsilon}\frac{\boldsymbol{\nu}-\mathbf{y}}{\|\boldsymbol{\nu}-\mathbf{y}\|_2} & \text{if } \|\boldsymbol{\nu}-\mathbf{y}\|_2^2 > \boldsymbol{\varepsilon} \\ \boldsymbol{\nu} & \text{if } \|\boldsymbol{\nu}-\mathbf{y}\|_2^2 \leq \boldsymbol{\varepsilon}\end{cases} \tag{9}$$

The resulting algorithm is summarized in Algorithm C-SALSA-2 [5570998].

3 EXPERIMENTAL RESULTS AND ANALYSIS

Experimental Setup

The reconstruction performance of UDCSMRI for various MR raw data, is analyzed from four aspects. Experimental raw data include complex-valued T2-weighted brain image (MR T2wBrain_slice27 of 256×256), water phantom [ning2013magnetic], real-valued MBA_T2_slice006, randomly selected

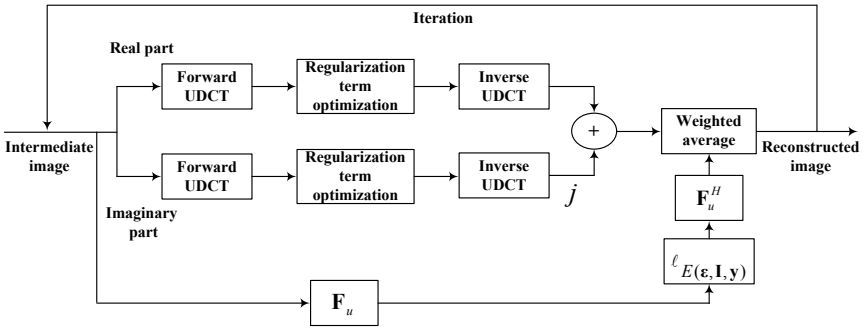

Figure 1. Framework of UDCT based CS MRI

AIDS dementia (slice 0-16), Brain Tumor (slice 0-23) and Normal aging (slice 0-53) (Courtesy of http://www.med.harvard.edu/AANLIB/home.html). Partial raw images and sampling schemes are shown in Fig.2. Computations are performed on a 64-bit Windows 7 operating system with an Intel Xeon E5 CPU at 2.80 GHz and 8 GB memory, MATLAB R2011b. Numerical metrics of quality assessment for reconstructed images are peak signal-to-noise ratio(PSNR) (in dB) and relative l_2 norm error(RLNE) [qu2012undersampled].

Comparison with Earlier Methods

The performance of UDCSMRI for images in Fig.2(a)-(c) is compared with that of TVCMRI, FCSA and WaTMRI. UDCT decomposition of $J = 1$, 12 directional sub-bands for each scale is adopted by Fig.2(a)-(b). For Fig.2(c), UDCT decomposition of $J = 3$, 12 directional sub-bands for each scale is used. The preset maximum iteration number for ADMM-2 is $K = 70$.

MR T2wBrain_slice27 reconstruction under 40% Cartesian sampling scheme is exhibited in Fig.3. Fig.3 indicates that reconstructed images under wavelet basis sparse regularization show severe pseudo-Gibbs phenomena, edge blur and aliasing. Whereas UDCSMRI with $\Phi = l_1$ (UDCSMRI(l_1)), UDCSMRI with $\Phi = TV$ (UDCSMRI(TV)) reconstructed images show clear edge details, the least aliasing and the lowest reconstructed error. Besides, UDCSMRI(TV) reconstructed image obtains the highest PSNR (39.10dB) and lowest RLNE(0.0684). These demonstrate that UDCSMRI performs preeminently in reconstructing T2wBrain_slice27.

For MBA_T2_slice006 reconstruction under Cartesian sampling scheme at 0.40 sampling rate, the reconstructed images PSNRs of TVCMRI, FCSA, WaTMRI, UDCSMRI(l_1) and UDCSMRI(TV) are 30.15dB, 31.08dB, 30.48dB, 36.01dB and 38.95dB, respectively. RLNEs are 0.1263, 0.1135, 0.1224, 0.0644 and 0.0459 separately. These indicate that UDCSMRI obtains the least reconstruction error.

Water phantom reconstructed results under 30.20% pseudo radial sampling scheme in Fig.4 indicate that TVCMRI, FCSA and WaTMRI can not reduce aliasing efficiently. While UDCSMRI(l_1) and UDCSMRI(TV) reconstructed images obtain clear edge structures. It is worth mentioning that reconstructed result in Fig.4(d) has better rhombic texture features and more clear directions than that in Fig.4(e). It means that UDCSMRI(l_1) performs better than UDCSMRI(TV) in reconstructing water phantom.

AIDS dementia (slice0-16), Brain Tumor (slice0-23) and Normal aging (slice0-53) reconstruction using Cartesian sampling at 0.40 sampling rate are implemented to further test the performance of UDCSMRI. PSNR and RLNE curves versus slices of UDCSMRI reconstruction, for AIDS dementia, Brain Tumor, Normal aging separately, are compared with those of TVCMRI, FCSA, WaTMRI. The comparison curves are exhibited in Fig.5. The statistical results in Fig.5 show that UDCSMRI can reconstruct original MR images from highly undersampled k-space with high probability among all the compared methods.

Sampled Data with Noise

The ability of UDCSMRI for handling noise is tested in this subsection. After random gaussian white noise with standard deviation of 10.2 is added to fully sampled k-space data, PSNRs for fully sampled reconstructed T2wBrain_slice27, MBA_T2_slice006 and water phantom are 29.87dB 28.94dB and 30.76dB separately. RLNEs are 0.1980, 0.1451 and 0.0609 separately. Table 1 shows numerical metrics for reconstructed T2wBrain_slice27 and MBA_T2_slice006 using sampling scheme in Fig.2(d) at 0.40 sampling rate, and reconstructed water phantom using sampling scheme in Fig.2(e) at 0.3020 sampling rate, respectively. In Table 1, UDCSMRI reconstructed results obtain the highest PSNR and lowest RLNE, indicating that UDCSMRI can eliminate noise efficiently. TV regularization constrained UDCSMRI performs better that l_1 regularization constrained UDCSMRI in eliminating noise in reconstructing images in Fig.2(a)-(b). While for reconstructing image in Fig.2(c) under

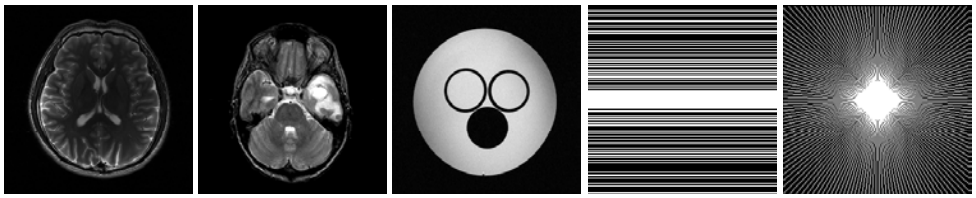

(a) (b) (c) (d) (e)

Figure 2. (a) MR T2wBrain_slice27, (b) MBA_T2_slice006, (c) Water phantom, (d) Cartesian sampling scheme and (e) Pseudo radial sampling scheme.

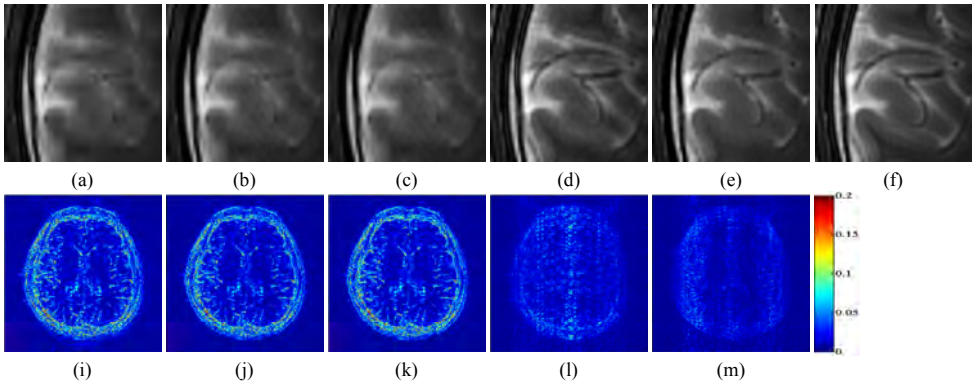

(a) (b) (c) (d) (e) (f)

(i) (j) (k) (l) (m)

Figure 3. T2wBrain_slice27 reconstruction with Cartesian sampling at 0.40 **sampling rate. (a)-(f) Amplified local regions of reconstructed images from TVCMRI, FCSA, WaTMRI, UDCSMRI(l_1), UDCSMRI(TV) and fully sampled k-space data separately, (g)-(k) Difference image between fully sampled MR image and TVCMRI, FCSA, WaTMRI, UDCSMRI(l_1), UDCSMRI(TV) reconstructed images with gray scale of [**0, 0.20**], respectively. PSNRs of TVCMRI, FCSA, WaTMRI, UDCSMRI(l_1), UDCSMRI(TV) reconstructed images are** 30.74**dB,** 31.29**dB,** 30.87**dB,** 36.41**dB and** 39.10**dB and RLNEs of them are** 0.1790**,** 0.1681**,** 0.1764**,** 0.0932 **and** 0.0684 **separately.**

(a) (b) (c) (d) (e) (f)

Figure 4. Pseudo radial sampling at 0.3020 **sampling rate. (a)-(f) Enlarged local regions of reconstructed water phantom from TVCMRI, FCSA, WaTMRI, UDCSMRI(l_1), UDCSMRI(TV) and fully sampled k-space data separately.**

noise, UDCSMRI(l_1) performs slightly better than UDCSMRI(TV).

Influences of Various Sparse Priors

Influences of various sparse priors to C-SALSA reconstruction performance without noise are discussed in this subsection, for reconstructing T2wBrain_slice27 and MBA_T2_slice006 under Cartesian sampling scheme at 0.40 sampling rate and water phantom under 30.20% pseudo radial sampling scheme. C-SALSA based on Daubechies wavelet basis, less redundant SFLCT(LRSFLCT) based C-SALSA, more redundant SFLCT(MRSFLCT) based C-SALSA, FDCT based C-SALSA and UDCSMRI reconstruction methods are compared in our work. In simulation, regularization parameters of compared methods are manually optimized for maximum PSNRs and minimum RLNEs. Table 2 and Table 3 exhibit reconstructed numerical indices using C-SALSA with $\Phi = l_1$ and $\Phi = TV$ separately. Table 2 exhibits clearly that reconstruction based on conventional sparse methods cannot efficiently eliminate artifacts and aliasing caused by Cartesian undersampling, particularly for wavelet and FDCT based C-SALSA. MRSFLCT based C-SALSA reconstructed images obtain slightly higher PSNRs and lower RLNEs separately than LRSFLCT based C-SALSA reconstructed images, indicating that increasing redundancy properly can improve the reconstruction quality to some extent. While UDCSMRI reconstructed images possess highest PSNRs and lowest RLNEs, indicating that UDCT performs best in sparsifying MR images and thus can lead to lower undersampling rate while

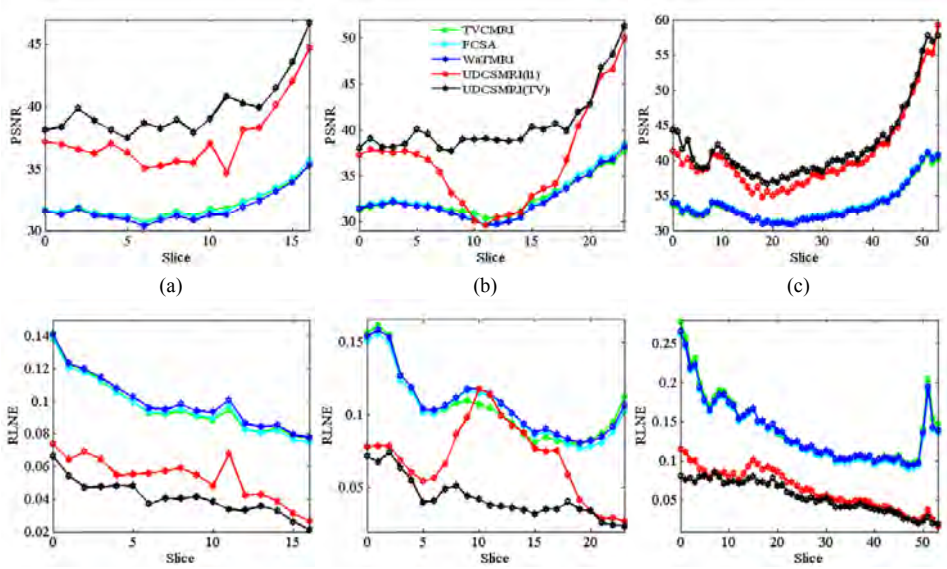

Figure 5. Cartesian sampling at 0.40 sampling rate. (a)-(c) PSNR versus slices for AIDS dementia, Brain Tumor and Normal aging, respectively. (d)-(f) RLNE versus slices for AIDS dementia, Brain Tumor and Normal aging, respectively.

Images & Sampling schemes	Indices	Methods				
		TVCMRI	FCSA	WaTMRI	UDCSMRI(l_1)	UDCSMRI(TV)
T2wBrain_slice27 & Cartesian	PSNR(dB)	28.79	28.67	28.38	31.84	**32.24**
	RLNE	0.2241	0.2272	0.2349	0.1577	**0.1507**
MBA_T2_slice006 & Cartesian	PSNR(dB)	29.63	29.57	29.32	31.36	**31.76**
	RLNE	0.1341	0.1351	0.1390	0.1099	**0.1049**
water phantom & pseudo	PSNR(dB)	12.62	9.43	9.38	**33.03**	32.80
	RLNE	0.4917	0.7102	0.7140	**0.0469**	0.0482

Table 1. Reconstructed images quality indices for sampled data with noise

Images & Sampling schemes	Indices	Sparse priors				
		Daubechies wavelet	LRSFLCT	MRSFLCT	FDCT	UDCT
T2wBrain_slice27 & Cartesian	PSNR(dB)	32.91	33.79	34.73	33.34	**36.41**
	RLNE	0.1395	0.1260	0.1131	0.1327	**0.0932**
MBA_T2_slice006 & Cartesian	PSNR(dB)	31.49	31.15	32.19	30.28	**36.01**
	RLNE	0.1083	0.1125	0.0998	0.1245	**0.0644**
water phantom & pseudo	PSNR(dB)	33.86	35.01	35.28	33.88	**35.74**
	RLNE	0.0426	0.0374	0.0362	0.0425	**0.0343**

Table 2. Various sparse priors with l_1 regularization

obtaining high-quality reconstruction. Table 3 shows similar reconstruction results in general. What worth mentioning is that MRSFLCT and LRSFLCT based C-SALSA ($\Phi = TV$) obtain the same numerical indices. Comparing Table 2 with Table 3, it can be concluded that l_1 regularization performs better than TV regularization for sparse transforms except UDCT.

Convergence Analysis

Convergence of UDCSMRI reconstruction is analyzed in this subsection. MSE versus ADMM-2 iteration number for reconstructing Fig.3(d) and (e), MBA_T2_slice006 under the same conditions and Fig.4(d) and (e) are exhibited in Fig.6. When iteration number reaches 25, MSE has already fell into minimal values. Conclusions are made that UDCSMRI(l_1) and UDCSMRI(TV) can obtain rapid convergence with very small MSEs.

4 CONCLUSIONS AND FUTURE WORK

A simple and efficient uniform discrete curvelet transform sparsity based CS MRI framework has been proposed in this paper. In this framework, UDCT obtains optimal structural sparsity, laying the foundation of high quality reconstruction from ill-posed linear in-

Images & Sampling schemes	Indices	Sparse priors				
		Daubechies wavelet	LRSFLCT	MRSFLCT	FDCT	UDCT
T2wBrain_slice27 & Cartesian	PSNR(dB)	28.45	31.40	31.41	30.82	**39.10**
	RLNE	0.2331	0.1659	0.1658	0.1774	**0.0684**
MBA_T2_slice006 & Cartesian	PSNR(dB)	26.80	30.44	30.44	30.08	**38.95**
	RLNE	0.1857	0.1221	0.1221	0.1274	**0.0459**
water phantom & pseudo	PSNR(dB)	31.11	33.01	33.01	33.01	**34.42**
	RLNE	0.0585	0.0470	0.0470	0.0470	**0.0400**

Table 3. Various sparse priors with TV regularization

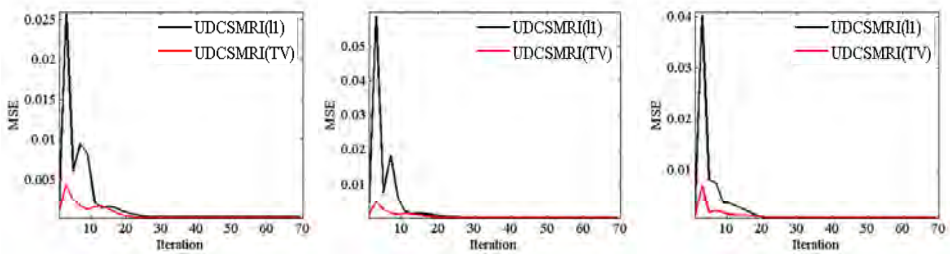

(a) (b) (c)

Figure 6. MSEs decline versus iteration. (a) Fig.3(d) and (e) reconstruction. (b) MBA_T2_slice006 reconstruction under the same conditions. (c) Fig.4(d) and (e) reconstruction.

verse problems. C-SALSA enforces optimized images transform sparsity and data fidelity at fast convergence speed. Experiments on various MR images illustrate the proposed method can achieve low reconstruction error among current CS MRI methods. The proposed method obtains preeminent reconstruction performance at the cost of doubling the amount of calculation due to handling the real part and imaginary part of complex-valued MR images separately, though. Thus, further improvements on the proposed method are subjects of ongoing research and can be made from the following three aspects: (1) Test and optimize the method on more datasets. (2) Expand the method to 3D dynamic MRI by adding sparsity regularization defined along the temporal axis. (3) Use partially parallel imaging(PPI) to accelerate imaging.

5 ETHICS STATEMENT

Brain image of MBA_T2_slice006, AIDS dementia, Brain Tumor and Normal aging were downloaded from http://www.med.harvard.edu/AANLIB/home.html.
The rest human images were acquired from healthy subjects under the approval of the Institute Review Board of Xiamen University and written consent was obtained from the participants. The data were analyzed anonymously.

6 ACKNOWLEDGMENTS

This work was partially supported by National Natural Science Foundation of China (Grant No.61175012, 61201421, 61201422), Science Foundation of Gansu Province of China (Grant No.1208RJZA265), Specialized Research Fund for the Doctoral Program of Higher Education of China (Grant No.20110211110026) and the Fundamental Research Funds for the Central Universities of China (Grant No.lzujbky-2013-k06, lzujbky-2015-108, lzujbky-2015-197).

7 REFERENCES

[1614066] Donoho, D.L. Compressed sensing. Information Theory, IEEE Transactions on, pp.1289-1306, 2006.

[baraniuk2007compressive] Baraniuk, R. Compressive sensing. IEEE signal processing magazine, 2007.

[lustig2007sparse] Lustig, M., Donoho, D., and Pauly, J.M. Sparse MRI: The application of compressed sensing for rapid MR imaging. Magnetic resonance in medicine, pp.1182-1195, 2007.

[4472246] Lustig, M., Donoho, D.L., Santos, J.M., and Pauly, J.M. Compressed Sensing MRI. Signal Processing Magazine, IEEE, pp.72-82, 2008.

[chen2010novel] Chen, Y.M., Ye, X.J, and Huang, F. A novel method and fast algorithm for MR image reconstruction with significantly under-sampled data. Inverse Problems and Imaging, pp.223-240, 2010.

[santos2006single] Santos, J.M., Cunningham, C.H., Lustig, M., Hargreaves, B.A., Hu, B.S., Nishimura, D.G., and Pauly, J.M. Single breath-hold whole-heart MRA using variable-density spirals at 3t. Magnetic resonance in medicine, pp.371-379, 2006.

[block2007undersampled] Block, K.T., Uecker, M., and Frahm, J. Undersampled radial MRI with multiple coils. Iterative image reconstruction us-

ing a total variation constraint. Magnetic resonance in medicine, pp.1086-1098, 2007.

[haldar2011compressed] Haldar, J.P., Hernando, D., and Liang, Z.P. Compressed-sensing MRI with random encoding. Medical Imaging, IEEE Transactions on, pp.893-903, 2011.

[huang2011efficient] Huang, J.Z., Zhang, S.T., and Metaxas, D. Efficient MR image reconstruction for compressed MR imaging. Medical Image Analysis, pp.670-679, 2011.

[huang2012compressed] Huang, J.Z., and Yang, F. Compressed magnetic resonance imaging based on wavelet sparsity and nonlocal total variation, in Biomedical Imaging (ISBI), 2012 9th IEEE International Symposium on, pp.968-971, 2012.

[1532309] Do, M.N., and Vetterli, M. The contourlet transform: an efficient directional multiresolution image representation. Image Processing, IEEE Transactions on, pp.2091-2106, 2005.

[da2006nonsubsampled] Da, C., Arthur, L., Zhou, J.P., and Do, M.N. The nonsubsampled contourlet transform: theory, design, and applications. Image Processing, IEEE Transactions on, pp.3089-3101, 2006.

[lu2006new] Lu, Y., and Do, M.N. A new contourlet transform with sharp frequency localization, in Image Processing, 2006 IEEE International Conference on, pp.1629-1632, 2006.

[candes2000curvelets] Candes, E.J., and Donoho, D.L. Curvelets: A surprisingly effective nonadaptive representation for objects with edges. DTIC Document, 2000.

[candes2006fast] Candes, E., Demanet, L., Donoho, D., and Ying, L.X. Fast discrete curvelet transforms. Multiscale Modeling & Simulation, pp.861-899, 2006.

[lim2010discrete] Lim, W.Q. The discrete shearlet transform: A new directional transform and compactly supported shearlet frames. Image Processing, IEEE Transactions on, pp.1166-1180, 2010.

[qin2013efficient] Qin, J., and Guo, W.H. An efficient compressive sensing MR image reconstruction scheme, in Biomedical Imaging (ISBI), 2013 IEEE 10th International Symposium on, pp.306-309, 2013.

[jung2009k] Jung, H., Sung, K., Nayak, K.S., Kim, E.Y., and Ye, J.C. k-t FOCUSS: A general compressed sensing framework for high resolution dynamic MRI. Magnetic Resonance in Medicine, pp.103-116, 2009.

[otazo2010combination] Otazo, R., Kim, D., Axel, L., and Sodickson, D.K. Combination of compressed sensing and parallel imaging for highly accelerated first-pass cardiac perfusion MRI. Magnetic Resonance in Medicine, pp.767-776, 2010.

[bilen2012high] Bilen, C., Wang, Y., and Selesnick, I.W. High-speed compressed sensing reconstruction in dynamic parallel MRI using augmented Lagrangian and parallel processing. Emerging and Selected Topics in Circuits and Systems, IEEE Journal on, pp.370-379, 2012.

[qu2010combined] Qu, X.B., Cao, X., Guo, D., Hu, C.W., and Chen, Z. Combined sparsifying transforms for compressed sensing MRI. Electronics letters, pp.121-123, 2010.

[lewicki2000learning] Lewicki, M.S., and Sejnowski, T.J. Learning overcomplete representations. Neural computation, pp.337–365, 2000.

[4494699] Rauhut, H., Schnass, K., and Vandergheynst, P. Compressed Sensing and Redundant Dictionaries. Information Theory, IEEE Transactions on, pp.2210-2219, 2008.

[ning2013magnetic] Ning, B., Qu, X.B., Guo, D., Hu, C.W., and Chen, Z. Magnetic resonance image reconstruction using trained geometric directions in 2D redundant wavelets domain and nonconvex optimization. Magnetic resonance imaging, pp.1611-1622, 2013.

[qu2012undersampled] Qu, X.B., Guo, D., Ning, B.D., Hou, Y.K., Lin, Y.L., Cai, S.H., and Chen, Z. Undersampled MRI reconstruction with patch-based directional wavelets. Magnetic resonance imaging, pp.964-977, 2012.

[dabov2007image] Dabov, K., Foi, A., Katkovnik, V., and Egiazarian, K. Image denoising by sparse 3-D transform-domain collaborative filtering. Image Processing, IEEE Transactions on, pp.2080-2095, 2007.

[adluru2010reconstruction] Adluru, G., Tasdizen, T., Schabel, M.C., and DiBella, E.V. Reconstruction of 3D dynamic contrast-enhanced magnetic resonance imaging using nonlocal means. Journal of Magnetic Resonance Imaging, pp.1217-1227, 2010.

[fang2010coherence] Fang, S., Ying, K., Zhao, L., and Cheng, J.P. Coherence regularization for SENSE reconstruction with a nonlocal operator (CORNOL). Magnetic Resonance in Medicine, pp.1413-1425, 2010.

[liang2011sensitivity] Liang, D., Wang, H.F., Chang, Y.C., and Ying, L. Sensitivity encoding reconstruction with nonlocal total variation regularization. Magnetic resonance in medicine, pp.1384-1392, 2011.

[wong2013sparse] Wong, A., Mishra, A., Fieguth, P., and Clausi, D.A. Sparse Reconstruction of Breast MRI Using Homotopic Minimization in a Region-

al Sparsified Domain. Biomedical Engineering, IEEE Transactions on, pp.743-752, 2013.

[akccakaya2011low] Akçakaya, M., Basha, T.A., Goddu, B., Goepfert, L.A., Kissinger, K.V., Tarokh, V., Manning, W.J., and Nezafat, R. Low-dimensional-structure self-learning and thresholding: Regularization beyond compressed sensing for MRI Reconstruction. Magnetic Resonance in Medicine, pp.756-767, 2011.

[qu2014magnetic] Qu, X.B., Hou, Y.K., Lam, F., Guo, D., Zhong, J.H., and Chen, Z. Magnetic resonance image reconstruction from undersampled measurements using a patch-based nonlocal operator. Medical image analysis, pp.843-856, 2014.

[rao1999affine] Rao, B.D., and Kreutz, D.K. An affine scaling methodology for best basis selection. Signal Processing, IEEE Transactions on, pp.187-200, 1999.

[candes2008enhancing] Candes, E.J., Wakin, M.B., and Boyd, S.P. Enhancing sparsity by reweighted l1 minimization. Journal of Fourier analysis and applications, pp.877-905, 2008.

[nocedal2006conjugate] Nocedal, J., and Wright, S.J. Conjugate gradient methods. Springer, 2006.

[aelterman2011augmented] Aelterman, J., Luong, Hiêp.Q., Goossens, B., Pižurica, A., and Philips, W. Augmented Lagrangian based reconstruction of non-uniformly sub-Nyquist sampled MRI data. Signal Processing, pp.2731-2742, 2011.

[van2008probing] Van Den Berg, E., and Friedlander, M.P. Probing the Pareto frontier for basis pursuit solutions. SIAM Journal on Scientific Computing, pp.890-912, 2008.

[yang2011alternating] Yang, J.F., and Zhang, Y. Alternating direction algorithms for l_1-problems in compressive sensing. SIAM journal on scientific computing, pp.250-278, 2011.

[Zhang2010] MATLAB software: http://www.caam.rice.edu/optimization l_1, 2010.

[yang2010fast] Yang, J.F., Zhang, Y., and Yin, W.T. A fast alternating direction method for TVL1-L2 signal reconstruction from partial Fourier data. Selected Topics in Signal Processing, IEEE Journal of, pp.288-297, 2010.

[becker2011nesta] Becker, S., Bobin, Jérôme., Candès, E.J. NESTA: a fast and accurate first-order method for sparse recovery. SIAM Journal on Imaging Sciences, pp.1-39, 2011.

[5570998] Afonso, M.V., Bioucas-Dias, J.M., and Figueiredo, M. A T. An Augmented Lagrangian Approach to the Constrained Optimization Formulation of Imaging Inverse Problems. Image Processing, IEEE Transactions on, pp.681-695, 2011.

[5443489] Nguyen, T.T., and Chauris, H. Uniform Discrete Curvelet Transform. Signal Processing, IEEE Transactions on, pp.3618-3634, 2010.

[esser2009applications] Esser, E. Applications of Lagrangian-based alternating direction methods and connections to split Bregman. CAM report, pp.31, 2009.

[natarajan1995sparse] Natarajan, B.K. Sparse approximate solutions to linear systems. SIAM journal on computing, pp.227-234, 1995.

[4303060] Chartrand, R. Exact Reconstruction of Sparse Signals via Nonconvex Minimization. Signal Processing Letters, IEEE, pp.707-710, 2007.

[ma2008efficient] Ma, S.Q., Yin, W.T., Zhang, Y., and Chakraborty, A. An efficient algorithm for compressed MR imaging using total variation and wavelets, in Computer Vision and Pattern Recognition, CVPR 2008, IEEE Conference on, pp.1-8, 2008.

[NIPS20124630] Chen C., and Huang, J.Z. Compressive Sensing MRI with Wavelet Tree Sparsity. Advances in Neural Information Processing Systems 25, pp.1115-1123, 2012.

[shin2013calibrationless] Shin, P.J., Larson, P.EZ., Ohliger, M.A., Elad, M., Pauly, J.M., Vigneron, D.B., and Lustig, M. Calibrationless parallel imaging reconstruction based on structured low-rank matrix completion. Magnetic Resonance in Medicine, 2013.

[chambolle2004algorithm] Chambolle, A. An algorithm for total variation minimization and applications. Journal of Mathematical imaging and vision, pp.89-97, 2004.

[Quwebsite2010] http://www.quxiaobo.org/index_publications.html, 2010.

[qu2002information] Qu, G.H., Zhang, D.L., and Yan, P.F. Information measure for performance of image fusion. Electronics letters, pp.313–315, 2002.

[liang2009accelerating] Liang, D., Liu, B., Wang, J.J., and Ying,L. Accelerating SENSE using compressed sensing. Magnetic Resonance in Medicine, pp.1574–1584, 2009.

[afonso2010fast] Afonso, M.V., Bioucas-Dias, José.M., and Figueiredo, Mário.AT. Fast image recovery using variable splitting and constrained optimization. Image Processing, IEEE Transactions on, pp.2345–2356, 2010.